Journal of The Electrochemical Society, **152** (2) G138-G143 (2005)
0013-4651/2005/152(2)/G138/6/$7.00 © The Electrochemical Society, Inc.

Barrier Capability of Hf-N Films with Various Nitrogen Concentrations Against Copper Diffusion in Cu/Hf-N/n$^+$-p Junction Diodes

Keng-Liang Ou,[a] Shi-Yung Chiou,[b] Ming-Hongn Lin,[c] and Ray-Quan Hsu[d,z]

[a]*Graduate Institute of Oral Sciences, College of Oral Medicine, Taipei Medical University, Taipei 110, Taiwan*
[b]*Department of Mold and Die Engineering and* [c]*Department of Mechanical Engineering, National Kaohsiung University of Applied Science, Kaohsiung 807, Taiwan*
[d]*Institute and Department of Mechanical Engineering, National Chiao-Tung University, Hsinchu 300, Taiwan*

Hafnium-based (Hf-N) films were prepared by reactive radio frequency (rf)-magnetron sputtering on blank silicon wafers. Nitrogen incorporation and phase transformation of hafnium-based thin film were analyzed by cross-sectional transmission electron microscopy, X-ray diffraction, and X-ray photoelectron spectroscopy. The as-deposited Hf film has a hexagonal close-packed structure and a low resistivity of 48.29 μΩ cm. With increasing nitrogen concentration of Hf-N film, phase transformations are identified as α-Hf → $HfN_{0.4}$ → ε-Hf_3N_2 → fcc-HfN. The thermal stability of the Cu/Hf-N/Si contact system is evaluated by thermal stressing at various annealing temperatures. For the Cu/Hf/Si contact system, the interfacial reaction between the Hf barrier layer and the Cu layer is observed after annealing at 550°C for 30 min, and copper-hafnium compounds form. Highly resistive copper silicide forms after annealing at 600°C for 30 min. The Hf barrier fails due to the reaction of Cu and the Hf barrier, in which Cu atoms penetrate into the Si substrate after annealing at high temperature. However, no copper-hafnium and copper silicide compounds are found for the Cu/$HfN_{0.47}$/Si contact system even after annealing at 650°C for 30 min. A hafnium diffusion barrier incorporated with nitrogen can suppress the formation of copper-hafnium compounds and copper penetration, and thus enhance the thermal stability of the barrier layer.
© 2005 The Electrochemical Society. [DOI: 10.1149/1.1850367] All rights reserved.

Manuscript submitted July 6, 2004; revised manuscript received July 21, 2004. Available electronically January 7, 2005.

The use of Cu in on-chip metallization of microelectronic devices has recently attracted considerable attention due to its lower electrical resistivity and higher electromigration resistance than aluminum. The use of copper, however, raises several problems. For instance, Cu cannot adhere well to most dielectric substrates and is highly reactive with most metals and semiconductors. Thus, thin-film adhesion promoters and diffusion barriers must be used to enhance the adhesion and inhibit diffusion in the Cu-based metallization. Refractory metals have been investigated for such applications. Among them, tantalum-based film has been proven to be one of the most useful barrier materials.[1-3] However, because the resistivities of TaN and Ta-Si-N films are about 200 and 625 μΩ cm, respectively, these materials are deemed unfavorable for use as low-resistivity diffusion barrier.[3-5] Therefore, new barrier materials with high thermal stability and low electrical resistivity are needed. Other refractory metals probably exhibit very favorable properties, and in particular, sputtered hafnium films have been subjected to preliminary evaluation.[6] Reactively sputtered HfN films with resistivity lower than 100 μΩ cm have been reported.[7,8] In addition, low-contact resistivity on the order of 10^{-8} Ω cm^2 can be obtained for Hf/n$^+$-Si systems.[9] In this work, properties of Hf-N films with various nitrogen contents were studied. Barrier capabilities against Cu diffusion were investigated for Cu/Hf/Si and Cu/Hf-N/Si contact systems.

Experimental

The barrier capability of Hf-N films against Cu diffusion was investigated using a structure of Cu/Hf-N/n$^+$-p junction diodes. The key feature of this experiment is the various nitrogen flow rates during sputtering of Hf-N film formation. First, p-type (100)-oriented Si wafers with a resistivity 6-9 Ω cm were used in this study. After standard RCA cleaning, the wafers were administered the local oxidation of silicon (LOCOS) process to define active regions. The n$^+$-p junctions were formed by As^+ implantation at 60 keV with a dose of 5×10^{15} cm^{-2} followed by the rapid thermal annealing (RTA) process at 1050°C for 30 s in N_2 ambient. After the contact windows were cleaned by dipping sample in HF, a reactively sputtered Hf-N film (50 nm) was deposited onto the active regions with various nitrogen flow ratios. In this paper, nitrogen flow ratio is defined as a ratio of N_2 partial flow to total gas flow (N_2 + Ar). Then Cu film with a thickness of 300 nm was deposited subsequently in the same sputtering system without breaking vacuum. During the sputtering, gas pressure was maintained at 6 mTorr with a power selected at 500 and 1500 W for Hf-N and Cu, respectively. Finally Cu and Hf-N layers were patterned by dilute HNO_3 and Cl_2 plasma, respectively, for the formation of Cu/Hf-N/n$^+$-p junction diodes.

To investigate the barrier capability of Hf-N films against Cu diffusion, the devices (Cu/Hf-N/n$^+$-p junction diode) were thermally annealed at a temperature ranging from 400 to 650°C for 30 min in a vacuum of 10^{-3} Torr. For electrical analyses, leakage current of the diodes was measured by an HP4145B semiconductor parameter-analyzer at a reverse bias of −5 V. After annealing at various temperatures for 30 min, the diode leakage current was measured. In addition, surface morphologies of the Hf-N films were analyzed by a Nanoscope III atomic force microscope (AFM) with a Si probe. The AFM probe was scanned over an area of 5×5 μm with 512 scans at 1 Hz scanning rate in tapping mode. Sheet resistance measurements were taken using a four-point probe system. Grazing incidence X-ray diffractometry (GIXRD) was used to identify the phases of the films. The compositions of the films were analyzed by X-ray photoemission spectroscopy (XPS) with a monochromatic Mg Kα source. The X-ray power was 250 W (15 kV at 16.7 mA). The XPS energy scale was calibrated by setting the binding energy of $Ag_{3d_{5/2}}$ line on clean silver to exactly 368.3 eV referenced to the Fermi level. The angle of incidence of the X-ray beam with the specimen normal was 45°. High-resolution scans were run for Hf and N using an X-ray beam with about a 15 nm diam. Furthermore, 300 nm thick Cu films were sputtered onto Hf-N films to investigate their ability to resist Cu diffusion. Cu/Hf-N/Si samples were annealed from 450 to 700°C in vacuum for 30 min to evaluate their barrier stability. The surface morphology of annealed Cu/barrier/Si was observed by scanning electron microscopy (SEM).

[z] E-mail: rqhsu@mail.nctu.edu.tw

Downloaded on 2014-04-26 to IP 140.113.38.11 address. Redistribution subject to ECS terms of use (see ecsdl.org/site/terms_use) unless CC License in place (see abstract).

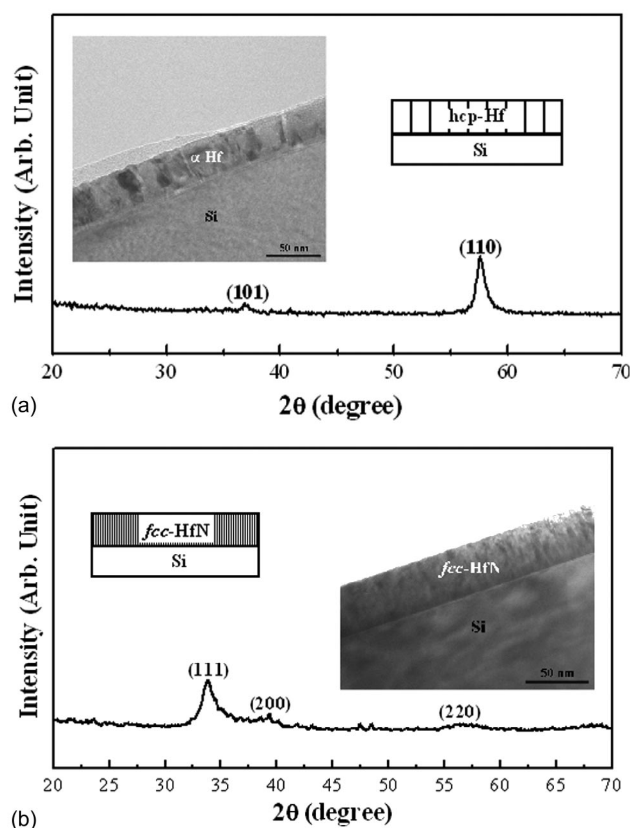

Figure 1. XRD patterns and XTEM images of the Hf and Hf-N films deposited on unpatterned silicon substrate: (a) Hf/Si and (b) Hf-N/Si system.

Compositions of failure sites were analyzed by energy-dispersive spectrometry (EDS) after removing both copper and barrier layers by wet-chemical solution. The interface microstructure was examined by transmission electron microscopy (TEM). Cross-sectional TEM (XTEM) samples were prepared by electron transparency by mechanical thinning followed by ion milling in a precision ion polishing system (PIPS).

Results and Discussion

Properties of the Hf-based thin films.—Figure 1 shows a series of X-ray diffraction (XRD) patterns and XTEM of Hf and Hf-N films deposited on unpatterned silicon substrates at various nitrogen flow rates. The XRD pattern of hafnium film on the unpatterned silicon wafer is shown as Fig. 1a. The (101) and (110) peaks confirm that the hafnium films on silicon substrates have a hexagonal close-packed (hcp) structure (α-Hf). The phase transformation of Hf-N films transforms from α-Hf to face-centered cubic (fcc)-HfN when an amount of nitrogen is added as shown in Fig. 1b. When the nitrogen flow rate increases to 3 sccm, the relatively sharp peaks of the fcc-HfN phase are observed for the Hf-N film, as shown in the curve of Fig. 1b. The XRD results in Fig. 1 clearly show that α-Hf and HfN phases form successively as nitrogen flow rate increases from 0 to 3.0 sccm. Furthermore, the as-deposited Hf film consists of fine (~30 nm) columnar grains, as shown in Fig. 1a; the finer grains are observed for the Hf-N film deposited at a nitrogen flow rate of 3 sccm, as shown in Fig. 1b.

XPS is performed to determine the nitrogen concentrations of the Hf-N films deposited at various nitrogen flow rates. The nitrogen content of the Hf-N film increases with the amount of nitrogen in the sputtering gas. The compositions of Hf-N films deposited at nitrogen flow rates of 1, 2, and 3 sccm are $HfN_{0.1}$, $HfN_{0.28}$, and $HfN_{0.47}$, respectively. Figure 2 offers consistent results regarding the critical

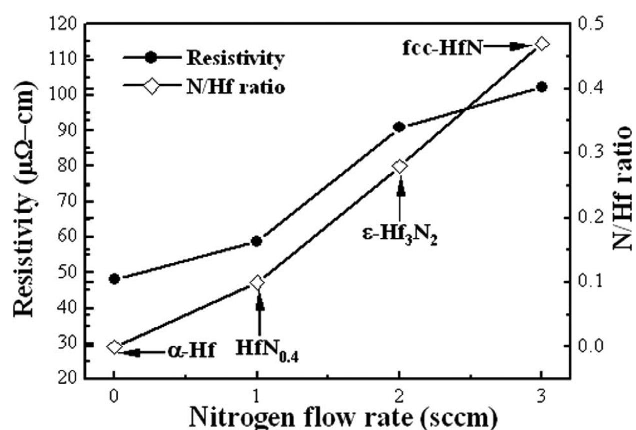

Figure 2. Electrical resistivity and composition (N/Hf atomic ratio) plots of Hf-based films deposited on silicon dioxide under various nitrogen flow rates.

nitrogen flow rates to form nitrogen-saturated $HfN_{0.1}$ (1 sccm), $HfN_{0.28}$ (2 sccm), and $HfN_{0.47}$ (3 sccm). Figure 2 also presents the electrical resistivity of Hf-N film as a function of nitrogen flow rate. The resistivity of the as-deposited film shows several interesting features. The electrical resistivity of the Hf film is 48.29 μΩ cm. Resistivity increases slightly when a small amount of nitrogen is added to the sputtering gas. The resistivity of the film increases to 90.8 μΩ cm when the nitrogen flow rate is 2 sccm. When more nitrogen is incorporated into the Hf film, the resistivity of the $HfN_{0.47}$ film increases to 102.31 μΩ cm. For comparison, the nitrogen flow rates (1, 2, and 3 sccm) dividing the four regions closely correspond to the flow rates of finding $HfN_{0.4}$, ε-Hf_3N_2, and fcc-HfN from XRD patterns. Moreover, the variations in resistivity are attributed to microstructure and phase transformation.

Thermal stability of Cu/Hf-N/Si contact systems.—Barrier capability of thin Hf and Hf-N films was investigated by evaluating the thermal stability of Cu/barrier (50 nm)/n^+-p junction diodes using electrical measurements. In this measurement, the leakage current densities were obtained from an average value of 25 samples and the diode area was 1000 × 1000 μm. Figure 3 illustrates the statistical distributions of reverse bias reverse current density for Cu/barrier (50 nm)/n^+-p junction diodes annealed at various temperatures. For the diodes without any heat-treatments (as-deposited), the leakage current densities remain stable (below 10 nA/cm^2) as nitrogen flow ratio is increased. However, the diode leakage increases with in-

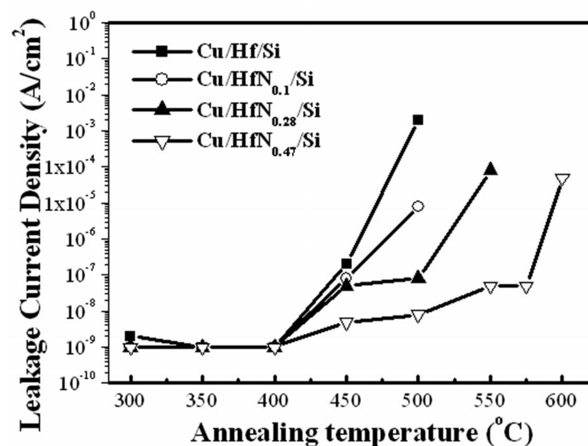

Figure 3. Variation in reverse current density of Cu/barrier/Si as a function of annealing temperature.

Downloaded on 2014-04-26 to IP 140.113.38.11 address. Redistribution subject to ECS terms of use (see ecsdl.org/site/terms_use) unless CC License in place (see abstract).

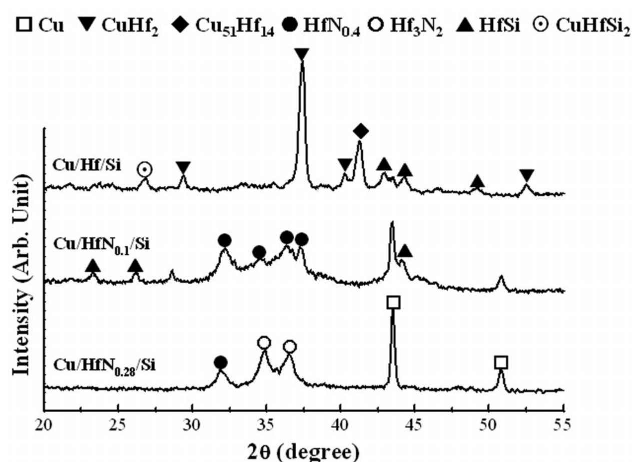

Figure 4. XRD patterns of Cu/Hf-N/Si contact systems after annealing at 550°C for 30 min.

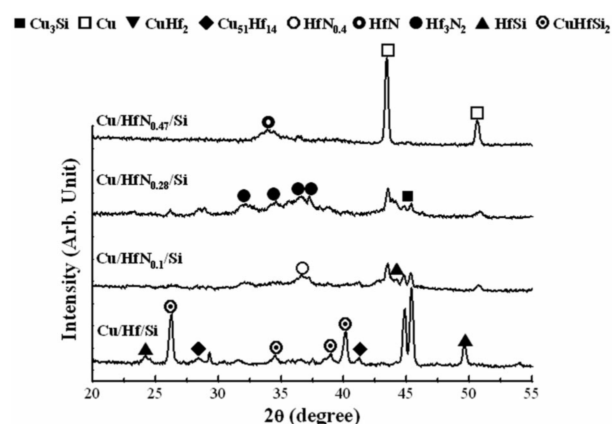

Figure 5. XRD patterns of Cu/Hf-N/Si contact systems after annealing at 600°C for 30 min.

creasing the annealing temperature, and most diodes are degraded after annealing at 600°C. As shown in Fig. 3, the leakage current densities initially decrease for 400°C annealing, and then increase with increasing the annealing temperatures. If we define a failure criterion with 10^{-6} A/cm^2, the Cu/Hf/n$^+$-p diodes remained stable after annealing at temperatures up to 450°C but suffered degradation at 500°C. It is reported that the barrier properties can be improved by adding impurities, such as N and O.[3,10-12] Figure 3 also shows the statistical distribution of reverse bias reverse current density for the Cu/$HfN_{0.1}$/n$^+$-p and Cu/$HfN_{0.28}$/n$^+$-p junction diodes annealed at various temperatures. For the diodes with 50 nm $HfN_{0.1}$ and $HfN_{0.28}$ barriers, the diodes remained stable after annealing at temperature up to 500 and 550°C, respectively. After annealing at 550°C, failure of the diodes was observed. Tsai *et al.* reported similar results. It was found that the diodes with 60 nm chemical vapor and physical vapor deposited TaN barriers would begin to deteriorate at 500 and 550°C, respectively.[13] It is revealed that barrier capability of Hf-N film is better than that of Hf film without nitrogen incorporation. However, the improvement of the barrier capability is limited. As nitrogen content increases, $HfN_{0.47}$ barrier was formed. The Cu/$HfN_{0.47}$/n$^+$-p diodes retained better electrical integrity after annealing at 550°C with lower leakage current densities. The $HfN_{0.47}$ films possess much better barrier performance than Hf, $HfN_{0.1}$, and $HfN_{0.28}$ barrier films. The improved barrier performance is attributed to finer crystallization, and interstitial effect is thought to induce microstructural variation and thereby improve barrier performance. It is reported that the microstructure within the barrier layer strongly affects the barrier performance because Cu diffuses through fast diffusion paths such as grain boundaries within the barrier layer.[3,13,14]

Figure 4 shows the XRD patterns of the Cu/Hf-N/Si samples after annealing at 550°C. Strong Cu(111) and weak Cu(200) peaks are observed in annealed Cu/$HfN_{0.1}$/Si and Cu/$HfN_{0.28}$/Si samples, implying that the Cu films prefer the ⟨111⟩ crystal orientation. Cu with a high ⟨111⟩ texture has been reported to exhibit higher electromigration resistance.[15] The diffraction peaks of α-Hf(101) and Cu(111) clearly disappear, and the $CuHf_2$ phase appears for the Cu/Hf/Si sample annealed at 550°C for 30 min. These results show that the interdiffusion of Cu and Hf induces the formation of Cu-Hf compounds. However, the Cu-Hf compounds are not observed in Cu/$HfN_{0.1}$/Si and Cu/$HfN_{0.28}$/Si samples after annealing at 550°C for 30 min. The strong diffraction peaks of $HfN_{0.4}$ and ε-Hf_3N_2 phases are observed. These results show that nitrogen incorporation in the Hf film can suppress the formation of Cu-Hf compound. Figure 5 shows XRD patterns of the Cu/Hf-N/Si samples after annealing at 600°C for 30 min. Strong Cu_3Si peaks are observed for the annealed Cu/Hf/Si sample. Strong Cu(111), weak Cu(200), and HfN(111) peaks are found in the XRD spectrum of annealed Cu/$HfN_{0.47}$/Si sample. The intensity of the HfN peak is lower. That is, it has a higher full width at half maximum (fwhm). The as-deposited $HfN_{0.47}$ barrier film has an amorphous-like structure.[16] Neither Cu-Si nor Cu-Hf compounds are observed after annealing at 600°C. The results indicate that the $HfN_{0.47}$ barrier is more effective in preventing Cu diffusion than the Hf barrier. Figure 6 shows XRD patterns of the Cu/$HfN_{0.47}$/Si samples after annealing at 650 and 700°C. The intensity of the HfN(111) peak increases obviously after 650°C annealing. This result reveals that annealing causes development of HfN crystals. Obvious Cu_3Si phases are found for Cu/$HfN_{0.47}$/Si samples annealed at 700°C for 30 min.

Figure 7 shows the SEM and cross-sectional TEM micrographs of Cu/Hf/Si after annealing at the temperature higher than the failure temperature. As shown in Fig. 7a, protrusions were observed on the surface, indicating a severe reaction of Cu/Hf/Si. Figure 7a also shows the EDS spectrum of the protrusion (denoted A). It revealed that the protrusion consisted of Cu and Si element and was a copper-rich region. These protrusions were presumably caused by Cu diffusion through the localized weak points in the barrier and reacting with underlying Si to form Cu_3Si. Similar phenomena were observed for Ta diffusion barriers by Wu *et al.*[14] Figure 7b shows the XTEM image of the Cu/Hf/Si sample after annealing at 600°C for 30 min. It is obvious that Hf silicide and Cu silicide were observed after annealing, and the interface of the sample was unclear. It indi-

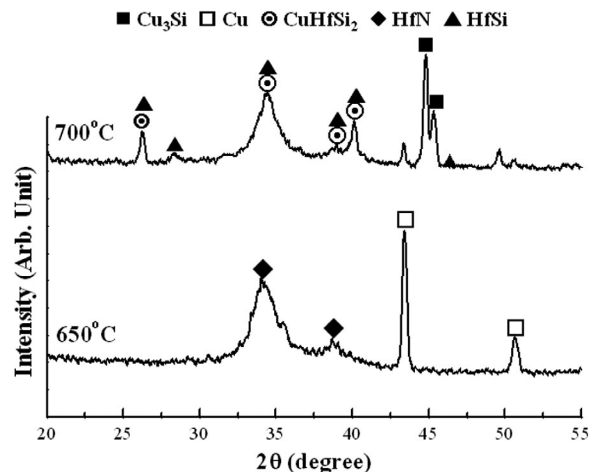

Figure 6. XRD patterns of Cu/$HfN_{0.47}$/Si contact systems after annealing at 650 and 700°C.

Downloaded on 2014-04-26 to IP 140.113.38.11 address. Redistribution subject to ECS terms of use (see ecsdl.org/site/terms_use) unless CC License in place (see abstract).

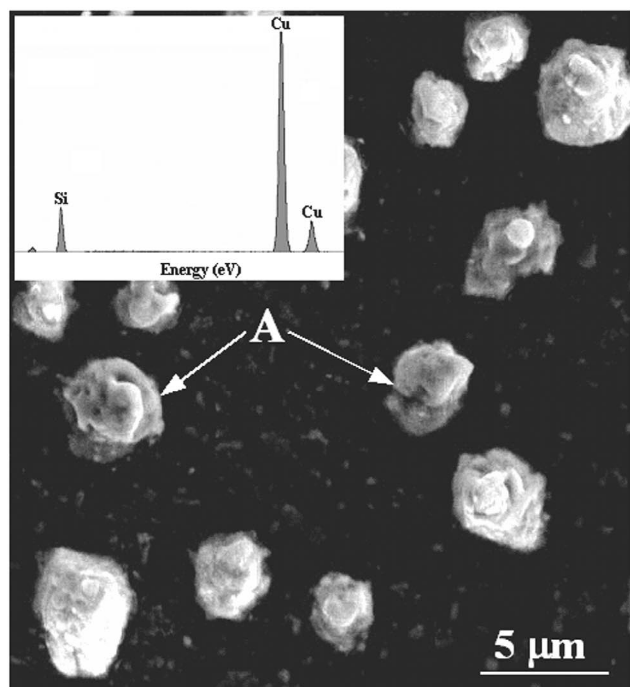

(a)

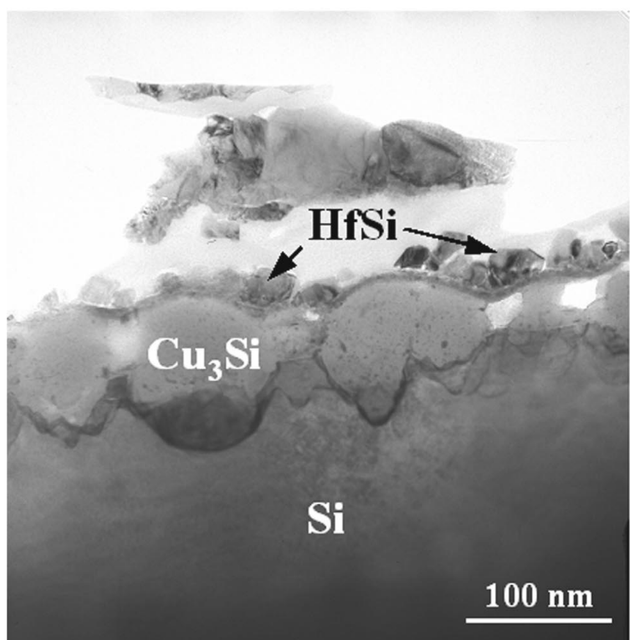

(b)

Figure 7. (a) SEM micrograph and EDS spectrum obtained from the precipitate of Cu/Hf/Si sample annealed at failure temperature and (b) XTEM micrograph of Cu/Hf/Si annealed at 550°C.

cates the degradation of the Hf barrier after annealing at 600°C for 30 min. The as-deposited Hf film consists of fine (∼30 nm) columnar grains. The degradation of the Hf barrier is attributed to the diffusion of Cu into the Si substrate through the columnar Hf barrier. Trapezoidal copper silicide spikes bounded by Si{111} and Si{001} planes were observed.[11] Figure 8 shows XTEM micrographs of $Cu/HfN_{0.47}/Si$ systems after annealing at various temperatures. Figure 8a shows the TEM image of the $Cu/HfN_{0.47}/Si$ sample after annealing at 650°C for 30 min. The multilayered structure is obvious. The diffraction ring patterns reveal HfN barrier film still possesses fcc structure and polycrystallinity after annealing at high temperature. However, the multilayered structure Cu/Hf-N/Si is retained. No Cu silicides are observed at the interface, demonstrating the excellent barrier properties. Figure 8b shows an XTEM image of 700°C-annealed $Cu/HfN_{0.47}/Si$. It is observed that the $HfN_{0.47}$ barrier layer is an enhanced crystalline structure having large columnar grains. Cu-Si compounds are observed on the Si substrate, demonstrating the Cu diffusion into the Si. In addition, the high-resolution XTEM, bright-field (BF) image, and selected area diffraction pattern (SADP) for $Cu/HfN_{0.47}/Si$ systems indicates the microstructure variations among the interlayers after annealing at 700°C, as shown Fig. 9. Figure 9a shows the microstructure in which the copper atoms diffuse through the $HfN_{0.47}$ layer and induces the formation of compounds adjacent to the Si substrate as noted with b_1, b_2, and b_3. The compounds of the inner layer are crystallized $CuHfSi_2$ from the analysis of diffraction patterns, as show in Fig. 9b, and the outer layer contains mixing phases of $HfN_{0.47}$ and HfSi, as shown in Fig. 9c. A high-resolution image of regions denoted as d_1 and c are shown in Fig. 10. These investigations of TEM are in agreement with the XRD results, which indicate the diffusion of Cu atoms through the $HfN_{0.47}$ layer, and that the formation of compounds containing Cu, Hf, and Si are the main causes of failure for $Cu/HfN_{0.47}/Si$ barrier layer.

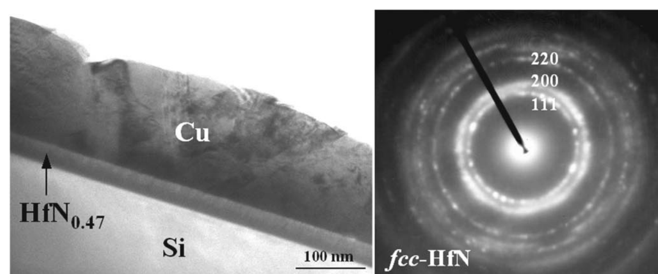

(a)

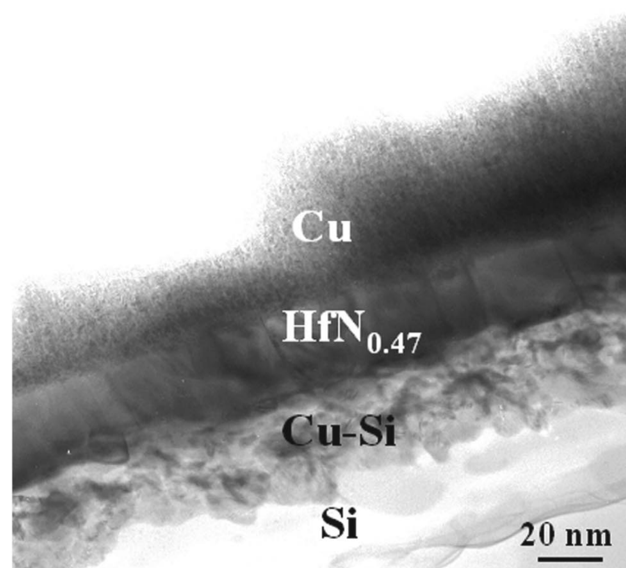

(b)

Figure 8. XTEM micrograph of $Cu/HfN_{0.47}/Si$ annealed at (a) 650 and (b) 700°C.

Failure mechanism of the Cu/Hf-N/Si system.—The XRD pat-

Downloaded on 2014-04-26 to IP 140.113.38.11 address. Redistribution subject to ECS terms of use (see ecsdl.org/site/terms_use) unless CC License in place (see abstract).

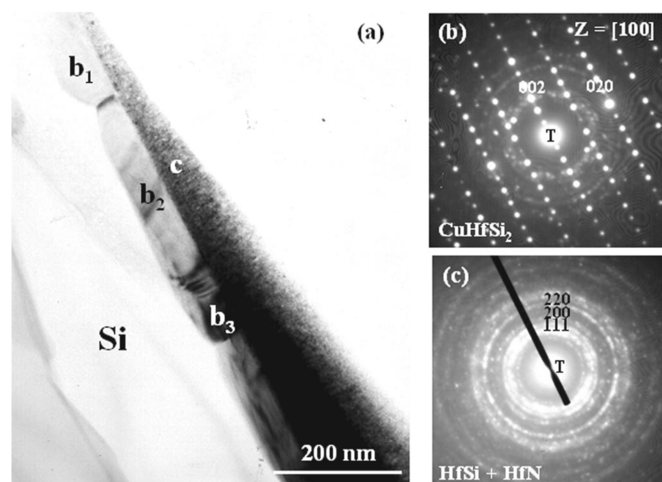

Figure 9. XTEM micrographs of $Cu/HfN_{0.47}/Si$ annealed at 700°C: (a) BF image and the corresponding SADP of (b) the grain denoted as b_1 and (c) the film denoted as c.

terns, XTEM, and reverse current density clearly reveal a difference between the failures of hafnium and hafnium nitride barriers. Hafnium film with nitrogen incorporation has improving barrier capability against copper diffusion. Nitrogen is not only incorporated into the hafnium to induce hafnium nitride, but is also present in interstitial positions at grain boundaries and lattice sites. The interstitial effect is thought to induce microstructural variation and thereby improve barrier performance. Figure 11 schematically shows cross sections of the interfacial structures of the Cu/Hf/Si, $Cu/HfN_{0.1}/Si$, $Cu/HfN_{0.28}/Si$, and $Cu/HfN_{0.47}/Si$ systems before and after annealing. Cu films on Hf-N barriers have a preferred {111} orientation. The as-deposited Hf barrier has an hcp-Hf structure with columnar grains, as shown in Fig. 11a. The formation of $CuHf_2$ and hafnium silicide is observed after annealing at 550°C for 30 min, revealing barrier degradation. The mechanism by which the barrier fails involves the sacrificial reaction of Hf with Cu and the motion of Cu through columnar Hf barrier to form Cu_3Si, as shown

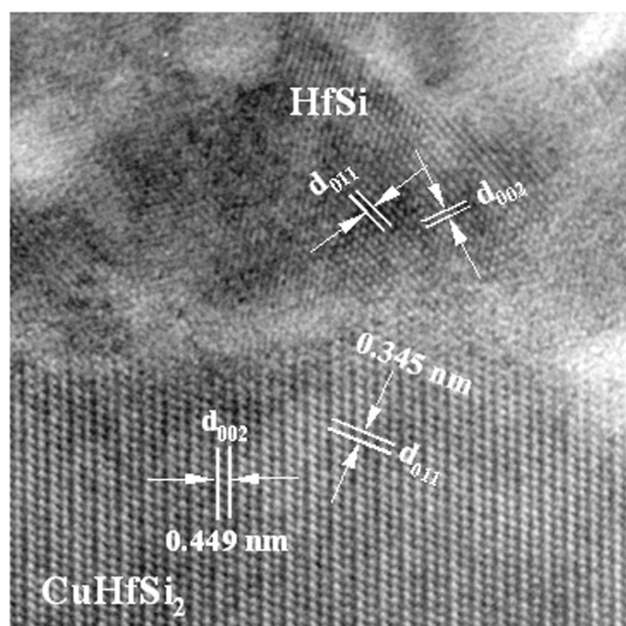

Figure 10. High-resolution TEM micrograph of $Cu/HfN_{0.47}$ interface in $Cu/HfN_{0.47}/Si$ sample after annealing at 700°C for 30 min.

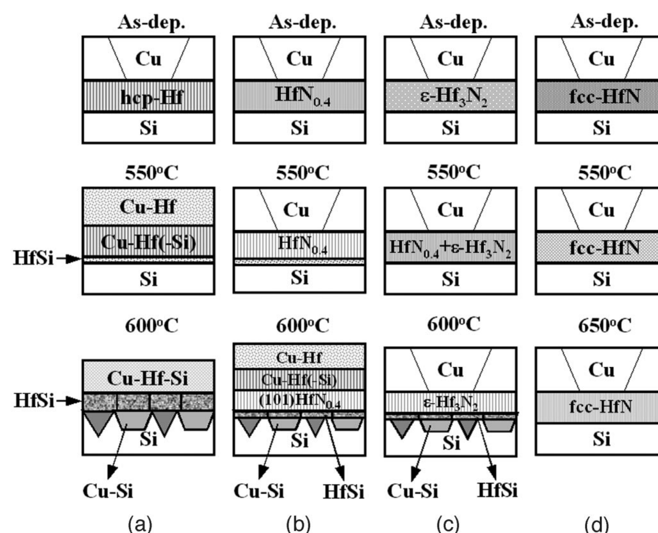

Figure 11. Schematic illustrations of the microstructures of (a) Cu/Hf/Si, (b) $Cu/HfN_{0.1}/Si$, (c) $Cu/HfN_{0.28}/Si$, and (d) $Cu/HfN_{0.47}/Si$ contact systems before and after annealing.

in Fig. 11a. The barrier capability of Hf film against Cu diffusion can be improved by incorporating nitrogen into Hf films using reactive sputtering. Adding impurities, such as N and O, has been reported to improve the barrier properties of refractory metals.[3,11,12] The as-deposited $HfN_{0.1}$, $HfN_{0.28}$, and $HfN_{0.47}$ barriers have the fine-grained $HfN_{0.4}$, ε-Hf_3N_2, and fcc-HfN phases, respectively, as shown in Fig. 11b-d. Neither Cu-Si nor Cu-Hf compounds are observed for the Cu/Hf-N/Si samples annealed at 550°C for 30 min, revealing better barrier performance than the Hf barrier. HfSi compound was formed after Cu/Hf/Si and $Cu/HfN_{0.1}/Si$ were annealed at 550°C for 30 min. The phenomenon was not observed in $Cu/HfN_{0.28}/Si$ and $Cu/HfN_{0.47}/Si$. It is evident that sheet resistance of Cu/Hf/Si and $Cu/HfN_{0.1}/Si$ increases after annealing at 550°C for 30 min (not shown). Furthermore, it is obvious that as nitrogen concentration increased, the interaction of Hf and Si is restrained. However, enhanced crystalline structure of the Hf-N barrier is found after annealing at 600°C. Cu_3Si compounds are observed for $Cu/HfN_{0.1}/Si$ and $Cu/HfN_{0.28}/Si$ systems after annealing at 600°C due to accelerating Cu diffusion through crystalline $HfN_{0.1}$ and $HfN_{0.28}$ barriers. However, Cu_3Si compounds are not observed for the $Cu/HfN_{0.47}/Si$ contact system annealed at 650°C. The microstructural transition of nitrogen-incorporated Hf film alleviates the Cu diffusion and hence, enhances the stability of the barrier and restrains the formation of copper-hafnium compounds. A Cu/Hf-N/Si contact system with high thermal stability is obtained.

Conclusion

Barrier capabilities against Cu diffusion were investigated for Cu/Hf/Si and Cu/Hf-N/Si contact systems. A thermally stable Cu/Si contact system, with a low-resistivity Hf-N diffusion barrier, is successfully demonstrated. The as-deposited Hf film has an hcp structure and a low resistivity of 48.29 $\mu\Omega$ cm. Phase transformations are identified as α-Hf $\rightarrow$ $HfN_{0.4}$ $\rightarrow$ ε-Hf_3N_2 $\rightarrow$ fcc-HfN with increasing nitrogen concentration of Hf-N film. Cu_3Si compounds are found for Cu/Hf/Si contact systems after annealing at 600°C. The mechanism by which the Hf barrier fails involves the sacrificial reaction of Hf with Cu and the motion of Cu through columnar Hf barrier to form Cu_3Si. The $Cu/HfN_{0.47}/Si$ contact system tolerates annealing at 650°C for 30 min without any reaction. Cu_3Si compounds are observed after annealing at 700°C due to accelerating Cu diffusion through crystalline Hf-N barrier. The $HfN_{0.47}$ layer with

Downloaded on 2014-04-26 to IP 140.113.38.11 address. Redistribution subject to ECS terms of use (see ecsdl.org/site/terms_use) unless CC License in place (see abstract).

low electrical resistivity is shown to perform effectively as a diffusion barrier and thus has potential for use in Cu metallization technology.

Acknowledgments

The work was financially supported by the National Science Council of the Republic of China under contract no. NSC 92-2314-B-038-037, and this study was sponsored by Taipei Medical University (TMU-AE1-B02).

Taipei Medical University assisted in meeting the publication costs of this article.

References

1. D. S. Yoon, H. K. Baik, and S. M. Lee, *J. Vac. Sci. Technol. B,* **17**, 174 (1999).
2. H. Ono, T. Nakano, and T. Ohta, *Appl. Phys. Lett.,* **64**, 1511 (1994).
3. W. L. Yang, W. F. Wu, D. G. Lin, C. C. Wu, and K. L. Ou, *Solid-State Electron.,* **45**, 149 (2001).
4. E. Kolawa, J. S. Chen, J. S. Reid, P. J. Pokela, and M. A. Nicolet, *J. Appl. Phys.,* **70**, 1369 (1991).
5. S. Shinkai, K. I. Yoshimoto, Y. Kitada, and K. Sasaki, *J. Appl. Phys.,* **39**, 5995 (2000).
6. I. Suni, M. Mäenpää, M. A. Nicolet, and M. Luomajärvi, *J. Electrochem. Soc.,* **130**, 1215 (1983).
7. S. Shinkai and K. Sasaki, *Jpn. J. Appl. Phys., Part 1,* **38**, 2097 (1999).
8. B. O. Johansson, J. E. Sundgren, and U. Helmersson, *J. Appl. Phys.,* **58**, 3112 (1985).
9. S. Zaima, N. Wakai, T. Yamauchi, and Y. Yasuda, *J. Appl. Phys.,* **74**, 6703 (1993).
10. B. O. Johansson, U. Helmersson, M. K. Hibbs, and J. E. Sundgren, *J. Appl. Phys.,* **58**, 3104 (1985).
11. K. Holloway, P. M. Fryer, C. Cabral, Jr., J. M. E. Harper, P. J. Bailey, and K. H. Kelleher, *J. Appl. Phys.,* **71**, 5433 (1992).
12. X. Sun, E. Kolawa, J. S. Chen, J. S. Reid, and M. A. Nicolet, *Thin Solid Films,* **236**, 347 (1993).
13. M. H. Tsai, S. C. Sun, C. E. Tsai, S. H. Chuang, and H. T. Chiu, *J. Appl. Phys.,* **79**, 6932 (1996).
14. W. F. Wu, K. L. Ou, C. P. Chou, and C. C. Wu, *J. Electrochem. Soc.,* **150**, G83 (2003).
15. Y. L. Chin, B. S. Chiou, and W. F. Wu, *Jpn. J. Appl. Phys., Part 1,* **39**, 6708 (2000).
16. S. Y. Chiou, K. L. Ou, W. F. Wu, C. P. Chou, and Y. M. Chang, in *Proceedings of the Symposium on Nano Device Technology*, p. 65, Hsinchu, Taiwan (2002).

Downloaded on 2014-04-26 to IP 140.113.38.11 address. Redistribution subject to ECS terms of use (see ecsdl.org/site/terms_use) unless CC License in place (see abstract).